Inorg. Chem. **2005**, *44*, 3215–3225

A New Strategy for the Improvement of Photophysical Properties in Ruthenium(II) Polypyridyl Complexes. Synthesis and Photophysical and Electrochemical Characterization of Six Mononuclear Ruthenium(II) Bisterpyridine-Type Complexes

Maria Abrahamsson,[†] Henriette Wolpher,[‡] Olof Johansson,[‡] Jan Larsson,[†] Mikael Kritikos,[§] Lars Eriksson,[§] Per-Ola Norrby,[||] Jonas Bergquist,[⊥] Licheng Sun,[‡,#] Björn Åkermark,[‡] and Leif Hammarström*,[†]

Department of Physical Chemistry, Uppsala University, Box 579, 751 23 Uppsala, Sweden, Departments of Organic Chemistry and Structural Chemistry, Stockholm University, 106 91 Stockholm, Sweden, Department of Chemistry, Technical University of Denmark, Building 201, Kemitorvet, DK-2800 Lyngby, Denmark, and Department of Analytical Chemistry, Uppsala University, Box 599, 751 24 Uppsala, Sweden

Received December 13, 2004

The synthesis and characterization of six ruthenium(II) bistridentate polypyridyl complexes is described. These were designed on the basis of a new approach to increase the excited-state lifetime of ruthenium(II) bisterpyridine-type complexes. By the use of a bipyridylpyridyl methane ligand in place of terpyridine, the coordination environment of the metal ion becomes nearly octahedral and the rate of deactivation via ligand-field (i.e., metal-centered) states was reduced as shown by temperature-dependent emission lifetime studies. Still, the possibility to make quasi-linear donor–ruthenium–acceptor triads is maintained in the complexes. The most promising complex shows an excited-state lifetime of $\tau = 15$ ns in alcohol solutions at room temperature, which should be compared to a lifetime of $\tau = 0.25$ ns for $[Ru(tpy)_2]^{2+}$. The X-ray structure of the new complex indeed shows a more octahedral geometry than that of $[Ru(tpy)_2]^{2+}$. Most importantly, the high excited-state energy was retained, and thus, so was the potential high reactivity of the excited complex, which has not been the case with previously published strategies based on bistridentate complexes.

Introduction

Ruthenium(II) polypyridyl complexes are widely used as photoactive components in many research areas such as photochemical solar energy conversion[1] and molecular electronics.[2] The trisbipyridine-type ruthenium(II) complexes are the most commonly used because of their favorable photophysical properties, which include a long excited-state lifetime (up to $\tau = 1$ μs) at ambient temperatures.[3] However, a linear arrangement for vectorial electron and energy transfers in multinuclear assemblies based on trisbidentate ruthenium(II) complexes is difficult to obtain.[4] One way to overcome this problem has recently been described by Sauvage and co-workers.[5] By linking two phenanthroline ligands, they managed to selectively prepare trisbidentate ruthenium(II) complexes, where substituents on the phenanthroline ligands were forced into a mutual trans relationship. Another approach, synthetically less demanding, involves the use of *trans*-$[Ru(bpy)_2(L-py)_2]^{2+}$ (bpy = 2,2′-bipyridine,

* Author to whom correspondence should be addressed. E-mail: Leifh@fki.uu.se.
[†] Department of Physical Chemistry, Uppsala University.
[‡] Department of Organic Chemistry, Stockholm University.
[§] Department of Structural Chemistry, Stockholm University.
[||] Technical University of Denmark.
[⊥] Department of Analytical Chemistry, Uppsala University.
[#] Present address: Department of Chemistry, Royal Institute of Technology, SE-100 44 Stockholm, Sweden.

(1) (a) Hagfeldt, A.; Grätzel, M. *Acc. Chem. Res.* **2000**, *33*, 269. (b) Meyer, T. J. *Acc. Chem. Res.* **1989**, *22*, 163. (c) Sun, L.; Hammarström, L.; Åkermark, B.; Styring, S. *Chem. Soc. Rev.* **2001**, *30*, 36.
(2) Barigelletti, F.; Flamigni, L. *Chem. Soc. Rev.* **2000**, *29*, 1.
(3) Juris, A.; Balzani, V.; Barigelletti, F.; Campagna, S.; Belser, P.; von Zelewsky, A. *Coord. Chem. Rev.* **1988**, *84*, 85.
(4) Sauvage, J.-P.; Collin, J.-P.; Chambron, J.-C.; Guillerez, S.; Coudret, C.; Balzani, V.; Barigelletti, F.; De Cola, L.; Flamigni, L. *Chem. Rev.* **1994**, *94*, 993.
(5) Pomeranc, D.; Heitz, V.; Chambron, J.-C.; Sauvage, J.-P. *J. Am. Chem. Soc.* **2001**, *123*, 12215.

10.1021/ic048247a CCC: $30.25
Published on Web 04/02/2005

Chart 1. Ligands Included in This Study

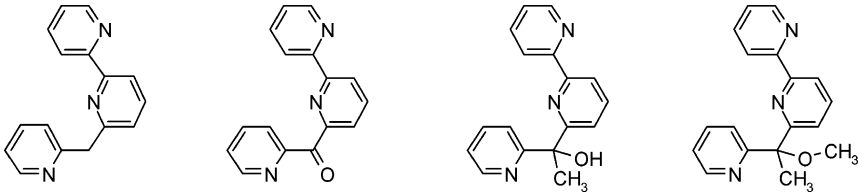

1 **2** **3** **4**

py = pyridine, and L = donor or acceptor group), but the resulting complexes are unstable.[6]

It was previously recognized that a linear arrangement could easily be obtained from the related bisterpyridine complexes by adding substituents to the 4′ positions of the terpyridine ligands.[4] Unfortunately, the use of these chromophores has been limited by the short excited-state lifetimes, $\tau = 0.25$ ns in the parent $[Ru(tpy)_2]^{2+}$ and $\tau = 0.95$ ns in $[Ru(ttpy)_2]^{2+}$ in alcohol solution and nitrile solvents, respectively (tpy is 2,2′:6′,2″-terpyridine and ttpy is 4′-tolyl-2,2′:6′,2″-terpyridine).[4] This is probably due to the weak ligand-field that is the result of the unfavorable bite angles of the 2,2′:6′,2″-terpyridine ligands.[4]

Approaches to extend the excited-state lifetimes of ruthenium(II) bisterpyridine complexes have mainly focused on modifications that affect the emitting ^{3}metal-to-ligand charge transfer (^{3}MLCT) states, thereby minimizing their interaction with higher-lying ^{3}MC states. This has been achieved by the use of substituents,[7] cyclometalating ligands,[8] and ligands with extended π systems.[9] Most of these attempts have resulted in a lowering of the ^{3}MLCT energy. A few recent studies have more specifically aimed at increasing the ligand-field strength by the use of strong σ-donor ligands,[7a−c] a strategy, however, that results in a concomitant decrease of the ^{3}MLCT state energy and, thus, limits the reactivity.

A complementary way to extend the excited-state lifetimes of ruthenium(II) bistridentate complexes should be to prepare ligands that can generate a more octahedral geometry and, thus, probably a stronger ligand field than that of the terpyridines. This would ideally lower the rate of population of the nonemissive ligand-field states without reducing the energy of the ^{3}MLCT state or decreasing the $Ru^{III/II}$ redox potentials, which are common problems associated with previous strategies. By linking 2,2′-bipyridine and pyridine by a single-carbon link, we have recently synthesized one such ligand (**1**) and the corresponding complex $[Ru(\mathbf{1})_2]^{2+}$.[10] A substantial increase in the excited-state lifetime relative to that of the parent $[Ru(tpy)_2]^{2+}$ was observed ($\tau = 15$ ns as compared to $\tau = 0.25$ ns), and the excited-state energy was only slightly reduced compared to that of $[Ru(tpy)_2]^{2+}$ ($E_{0-0} = 2.03$ eV as compared to $E_{0-0} = 2.07$ eV). To get an understanding of which effects might be involved, we have now prepared a series of related ligands and complexes and investigated their photophysical properties in some detail.

Results

Synthesis. The ligand [6-(2,2′-bipyridyl)]-(2-pyridyl)-methane (**1**) was prepared by reduction of the corresponding ketone (**2**).[11] Because it seemed interesting to study the effect of substituents on the bridging carbon, it was decided to also prepare the related ligands **3** and **4** and study the complexes of these ligands. All of the ligands included in this study are shown in Chart 1. The ligand 1-[6-(2,2′-bipyridyl)]-1-(2-pyridyl)-ethanol (**3**) was prepared by the addition of 6-lithio-2,2′-bipyridine to 2-acetylpyridine at −78 °C. Selective alkylation of the hydroxyl group to give **4** was achieved by the deprotonation of **3** with potassium *tert*-butoxide in THF followed by the addition of methyliodide.

The synthesis of the ruthenium(II) complexes (Chart 2) was performed following standard procedures. Refluxing the ligands **1**, **2**, **3**, and **4** with 1 equiv of $Ru(ttpy)(DMSO)Cl_2$ in ethanol or an ethanol/water mixture (2:1) gave, after chromatography (silica gel, CH_3CN/H_2O, KNO_3 mixtures) and anion metathesis, the corresponding $[Ru(ttpy)(X)][PF_6]_2$ complexes. For $[Ru(ttpy)(\mathbf{3})]^{2+}$, two different donor sets are conceivable. Either pyridine (N_6) or hydroxyl (N_5O) coordination are possible, but only pyridine coordination was observed under these conditions. The homoleptic complexes $[Ru(\mathbf{1})_2][PF_6]_2$ and $[Ru(\mathbf{4})_2][PF_6]_2$ were prepared in an analogous way from 2 equiv of **1** or **4**, respectively, and $Ru(DMSO)_4Cl_2$. All of the complexes were characterized by ^{1}H NMR, ESI-MS (or MALDI-TOF), and elemental analy-

(6) Coe, B. J.; Friesen, D. A.; Thompson, D. W.; Meyer, T. J. *Inorg. Chem.* **1996**, *35*, 4575.

(7) (a) Duati, M.; Fanni, S.; Vos, J. G. *Inorg. Chem. Commun.* **2000**, *3*, 68. (b) Duati, M.; Tasca, S.; Lynch, F. C.; Bohlen, H.; Vos, J. G.; Stagni, S.; Ward, M. D. *Inorg. Chem.* **2003**, *42*, 8377. (c) Indelli, M. T.; Bignozzi, C. A.; Scandola, F.; Collin, J.-P. *Inorg. Chem.* **1998**, *37*, 6084. (d) Constable, E. C.; Cargill Thompson, A. M. W.; Armaroli, N.; Balzani, V.; Maestri, M. *Polyhedron* **1992**, *11*, 2707. (e) Maestri, M.; Armaroli, N.; Balzani, V.; Constable, E. C.; Cargill Thompson, A. M. W. *Inorg. Chem.* **1995**, *34*, 2759. (f) Wang, J.; Fang, Y.-Q.; Hanan, G. S.; Loiseau, F.; Campagna, S. *Inorg. Chem.* **2005**, *44*, 5. (g) Medlycott, E. A.; Hanan, G. S. *Chem. Soc. Rev.* **2005**, *34*, 133.

(8) (a) Beley, M.; Collin, J.-P.; Louis, R.; Metz, B.; Sauvage, J.-P. *J. Am. Chem. Soc.* **1991**, *113*, 8521. (b) Beley, M.; Collin, J.-P.; Sauvage, J.-P. *Inorg. Chem.* **1993**, *32*, 4539. (c) Collin, J.-P.; Beley, M.; Sauvage, J.-P.; Barigelletti, F. *Inorg. Chim. Acta.* **1991**, *186*, 91.

(9) (a) Ceroni, P.; Credi, A.; Balzani, V.; Campagna, S.; Hanan, G. S.; Arana, C. R.; Lehn, J.-M. *Eur. J. Inorg. Chem.* **1999**, 1409. (b) Encinas, S.; Flamigni, L.; Barigelletti, F.; Constable, E. C.; Housecroft, E. C.; Schofield, E. R.; Figgemeier, E.; Fenske, D.; Neuburger, M.; Vos, J. G.; Zehnder, M. *Chem. Eur. J.* **2002**, *8*, 137. (c) Fang, Y.-Q.; Taylor, N. J.; Hanan, G. S.; Loiseau, F.; Passalacqua, R.; Campagna, R.; Nierengarten, H.; Van Dorsselaer, A. *J. Am. Chem. Soc.* **2002**, *124*, 7912. (d) Hammarström, L.; Barigelletti, F.; Flamigni, L.; Indelli, M. T.; Armaroli, N.; Calogero, G.; Guardigli, M.; Sour, A.; Collin, J.-P.; Sauvage, J.-P. *J. Phys. Chem. A* **1997**, *101*, 9061. (e) Hissler, M.; El-ghayoury, A.; Harriman, A.; Ziessel, R. *Angew. Chem., Int. Ed.* **1998**, *37*, 1717.

(10) Wolpher, H.; Johansson, O.; Abrahamsson, M.; Kritikos, M.; Sun, L.; Åkermark, B. *Inorg. Chem. Commun.* **2004**, *7*, 337.

(11) Parks, J. E.; Wagner, B. E.; Holm, R. H. *J. Organomet. Chem.* **1973**, *56*, 53.

Chart 2. Structures of the Complexes. All Complexes Were Isolated as PF_6^- Salts

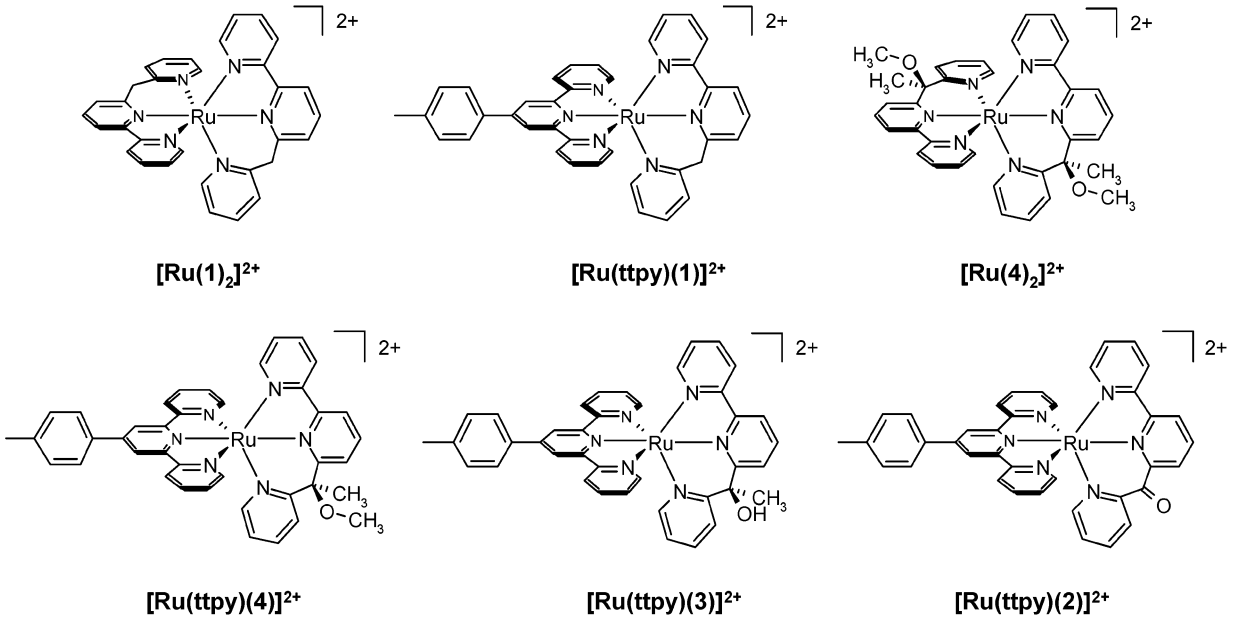

ses, which were in accordance with the assigned structures. In contrast to the homoleptic complex $[Ru(\mathbf{1})_2]^{2+}$ (see below), complex $[Ru(\mathbf{4})_2]^{2+}$ showed dynamic behavior in the ^{1}H NMR spectrum, and therefore, no attempt was made to isolate the corresponding homoleptic complex of ligand **3**. The dynamic behavior was indicated by several broad NMR peaks in the region corresponding to the protons of the methoxy groups. On cooling, these peaks changed in a very complex way, which we were unable to interpret in a satisfactory manner. The emission spectra and lifetime for this complex were also poorly defined, and this complex was, therefore, not further investigated.

^{1}H NMR Spectroscopy. The ^{1}H NMR characterizations of the complexes $[Ru(\mathbf{1})_2]^{2+}$, $[Ru(ttpy)(\mathbf{1})]^{2+}$, $[Ru(ttpy)(\mathbf{2})]^{2+}$, $[Ru(ttpy)(\mathbf{3})]^{2+}$, and $[Ru(ttpy)(\mathbf{4})]^{2+}$ were achieved by one- and two-dimensional NMR techniques.

The coordination of 2 equiv of **1** to Ru^{II} produced complex $[Ru(\mathbf{1})_2]^{2+}$, which was of C_2 symmetry, isolated as a racemic mixture. The two methylene protons in **1** that are enantiotopic in the free ligand become diastereotopic in the complex and appear as a pair of doublets. In accordance with the high symmetry of $[Ru(\mathbf{1})_2]^{2+}$, only 11 aromatic proton signals appeared in the NMR spectrum.

The ^{1}H NMR spectra of $[Ru(ttpy)(\mathbf{3})]^{2+}$ and $[Ru(ttpy)(\mathbf{4})]^{2+}$ (C_1 symmetry) consist of 23 resonances in the aromatic region. An assignment was possible from COSY and NOESY experiments. The chemical shift of the H_5 proton in the isolated pyridine is positioned the most upfield of all of the pyridine proton resonances. In addition, the H_3 proton of the isolated pyridine shows a NOE to the adjacent methyl group. On the basis of this, we were able to assign all of the proton resonances of the bipyridylpyridyl-type ligand. The protons of the 2,2′:6′,2″-terpyridine ligand were assigned on the basis of a NOE between the H_6 proton on one terminal pyridine ring and the methyl group of the bipyridylpyridyl ligands **3** and **4** (Figure 1).

For $[Ru(ttpy)(\mathbf{1})]^{2+}$ and $[Ru(ttpy)(\mathbf{2})]^{2+}$ (C_S symmetry), the terminal pyridines of the ttpy ligand are equivalent by symmetry on the NMR time scale, and only 18 aromatic proton resonances appear. A comparison of the spectra of $[Ru(ttpy)(\mathbf{1})]^{2+}$ and $[Ru(ttpy)(\mathbf{3})]^{2+}$ reveals some important differences (Figure 1). The H_6 protons of the ttpy ligand in $[Ru(ttpy)(\mathbf{1})]^{2+}$ appear at 7.63 ppm as a result of the shielding these protons experience from the central pyridine of the orthogonal ligand **1**. In $[Ru(ttpy)(\mathbf{3})]^{2+}$, however, the H_6 proton in the ttpy ligand that interacts with the methyl group of the bipyridylpyridyl ligand **3** resonates at 8.10 ppm, suggesting a position of the H_6 proton further away from the central pyridine in **3**. In contrast, the other H_6 proton on the opposite side of the ttpy ligand in $[Ru(ttpy)(\mathbf{3})]^{2+}$ is strongly shielded and resonates at ∼7.1 ppm. This is also supported by the X-ray crystal determination and molecular mechanics (MM) calculations of $[Ru(ttpy)(\mathbf{3})]^{2+}$ discussed below. In the complex $[Ru(ttpy)(\mathbf{4})]^{2+}$, the effect is not as pronounced as it is in $[Ru(ttpy)(\mathbf{3})]^{2+}$ and the H_6 protons of the ttpy ligand appear at 7.80 and 7.47 ppm, respectively.

X-ray Crystallography. The anticipated meridional coordination of 2 equiv of **1** to ruthenium(II) was confirmed by the crystal structure of $[Ru(\mathbf{1})_2]^{2+}$ (Figure 2a). The complex crystallized in the triclinic space group $P\bar{1}$ with two formula units per unit cell; selected bond lengths and bond angles are given in Tables 1 and 2. The ruthenium−nitrogen (bpy) bond lengths are within 2.034−2.059 Å {cf. (Ru−N) = 2.056 Å in $[Ru(bpy)_3]^{2+}$},[12] whereas the ruthenium−nitrogen (py) bond lengths are longer, 2.109 and 2.114 Å. Similar Ru−N bond distances have been previously observed in Ru−pyridine complexes {mean Ru−N (py) = 2.10 Å in *cis*-$[Ru(bpy)_2(py)_2]^{2+}$ and 2.12 Å in $[Ru(py)_6]^{2+}$}.[13]

(12) Rillema, D. P.; Jones, D. S.; Woods, C.; Levy, H. A. *Inorg. Chem.* **1992**, *31*, 2935.
(13) (a) Hitchcock, P. B.; Seddon, K. R.; Turp, J. E.; Yousif, Y. Z.; Zora, J. A.; Constable, E. C.; Wernberg, O. *J. Chem. Soc., Dalton Trans.* **1998**, 1837. (b) Templeton, J. L. *Inorg. Chem.* **1979**, *101*, 4906.

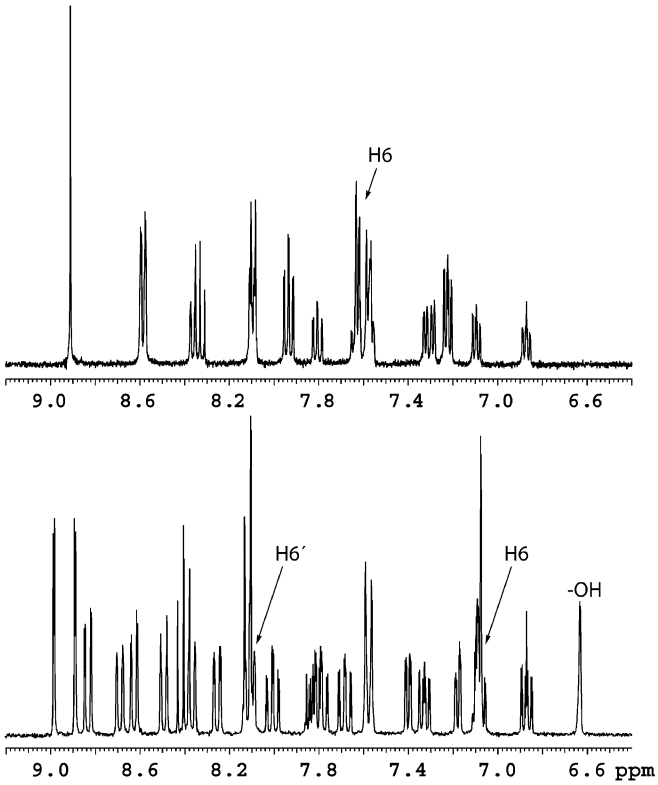

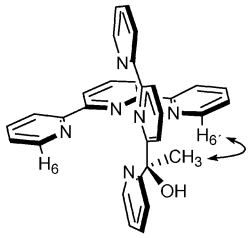

Figure 1. Left: NMR spectra of $[Ru(ttpy)(\mathbf{1})]^{2+}$ (top) and $[Ru(ttpy)(\mathbf{3})]^{2+}$ (bottom) recorded in CD_3CN (298 K, 300 MHz). Right: Interligand interaction in $[Ru(ttpy)(\mathbf{3})]^{2+}$. Ru and the *p*-tolyl group are omitted for clarity.

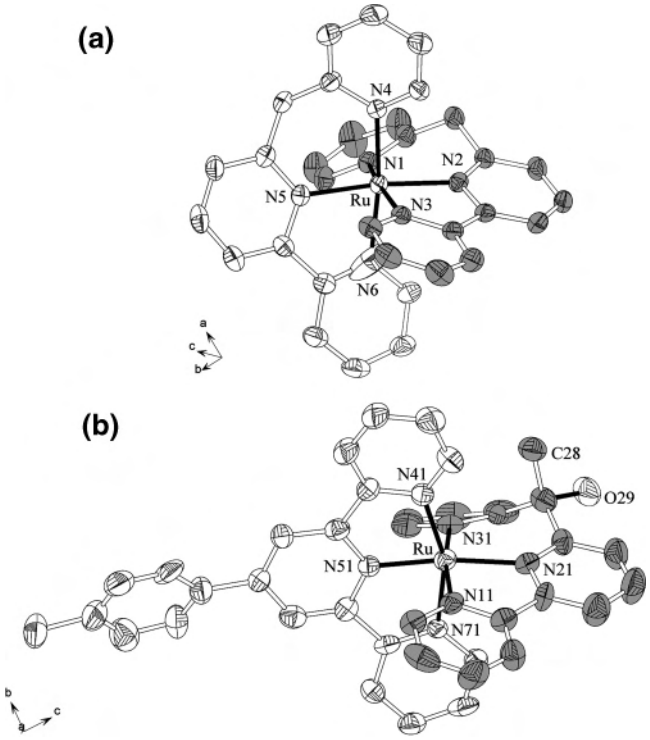

Figure 2. (a) ORTEP view (30% probability ellipsoids) of $[Ru(\mathbf{1})_2]^{2+}$. (b) ORTEP view (30% probability ellipsoids) of $[Ru(ttpy)(\mathbf{3})]^{2+}$.

Table 1. Selected Crystal Data for $[Ru(\mathbf{1})_2]^{2+}$ and $[Ru(ttpy)(\mathbf{3})]^{2+}$

empirical formula	$C_{36}H_{36}N_6OP_2F_{12}Ru$	$C_{39}H_{31}Cl_2N_6O_9Ru$
fw	959.72	915.15
cryst syst	triclinic	triclinic
space group	$P\bar{1}$ (No. 2)	$P\bar{1}$ (No. 2)
a, Å	12.549(2)	9.441(2)
b, Å	12.826(2)	11.816(2)
c, Å	13.283(3)	19.134(4)
α, deg	89.84(2)	86.05(2)
β, deg	70.16(2)	76.49(2)
γ, deg	77.36(2)	81.55(2)
V, Å^3	1956.2(5)	2051.8(6)
Z	2	2
ρ_{calc}, g cm^{-3}	1.629(1)	1.481(1)
temp, K	293	293
μ (MoKα), (mm^{-1})	0.579	0.593
N(meas), *N*(uniq), *R*(int)	15314, 7099, 0.1089	24650, 6803, 0.2295
N(obs), *N*(par), *S*	4579, 526, 0.956	2358, 517, 0.783
R1, wR2, [$I > 2\sigma(I)$]	0.0504, 0.1134	0.0919, 0.2136
$\Delta\rho_{min}$, $\Delta\rho_{max}$ (e/Å^3)	−0.87, 0.92	−0.645, 1.343

Table 2. Selected Bond Lengths (Å) and Angles (deg) for $[Ru(\mathbf{1})_2]^{2+}$

Ru1−N1	2.114(5)	Ru1−N4	2.109(5)
Ru1−N2	2.043(4)	Ru1−N5	2.034(4)
Ru1−N3	2.059(4)	Ru1−N6	2.054(5)
N1−Ru1−N2	91.4(2)	N2−Ru1−N6	95.45(2)
N1−Ru1−N3	168.3(2)	N3−Ru1−N4	89.1(2)
N1−Ru1−N4	98.9(2)	N3−Ru1−N5	95.7(2)
N1−Ru1−N5	92.4(2)	N3−Ru1−N6	83.8(2)
N1−Ru1−N6	89.5(2)	N4−Ru1−N5	92.7(2)
N2−Ru1−N3	79.67(2)	N4−Ru1−N6	168.4(2)
N2−Ru1−N4	92.39(2)	N5−Ru1−N6	78.8(2)
N2−Ru1−N5	173.06(2)		

The N−Ru−N angles of the bipyridyl units [N(2)−N(3) and N(5)−N(6)], just under 80°, are unremarkable. Because of the inserted carbon atom between the central pyridine and the isolated pyridine in **1**, these angles are substantially greater [N(1)−N(2) = 91.4° and N(4)−N(5) = 92.7°], resulting in ligand bite angles that are closer to octahedral [N(1)−N(3) = 168.3°, N(4)−N(6) = 168.4°, and N(2)−N(5) = 173.06°] compared to those of the parent $[Ru(tpy)_2]^{2+}$, which has N−Ru−N angles of 158.4°, 159.1°, and 178.8°.[14]

Table 3. Selected Bond Lengths (Å) and Angles (deg) for $[Ru(ttpy)(\mathbf{3})]^{2+}$

Ru1−N11	2.016(12)	Ru1−N41	2.088(11)
Ru1−N21	2.086(11)	Ru1−N51	1.935(10)
Ru1−N31	2.108(12)	Ru1−N71	2.049(10)
N11−Ru1−N21	80.3(4)	N51−Ru1−N21	172.2(4)
N11−Ru1−N31	168.5(4)	N51−Ru1−N31	93.9(5)
N11−Ru1−N41	90.1(4)	N51−Ru1−N41	78.9(4)
N11−Ru1−N71	88.4(4)	N51−Ru1−N71	79.4(4)
N21−Ru1−N31	91.6(5)	N71−Ru1−N21	95.7(4)
N21−Ru1−N41	105.7(4)	N71−Ru1−N41	158.1(4)
N41−Ru1−N31	100.0(4)	N71−Ru1−N31	84.3(4)
N51−Ru1−N11	93.5(4)		

The heteroleptic complex $[Ru(ttpy)(\mathbf{3})]^{2+}$ (ClO_4^- salt) also crystallized in a triclinic unit cell of the $P\bar{1}$ space group (Figure 2b). The ruthenium−nitrogen bond lengths are reminiscent of complexes $[Ru(\mathbf{1})_2]^{2+}$ and $[Ru(tpy)_2]^{2+}$, respectively (Table 3). The bond angles, however, are significantly changed from those of the parent $[Ru(tpy)_2]^{2+}$ complex, as shown by the N−Ru−N angles between the central pyridine of **3** and the terminal pyridine rings of the ttpy ligand [N(21)−N(41) = 105.7° and N(21)−N(71) = 95.7°]. This originates from the steric interaction between the methyl group of **3** and the H_6 proton of the ttpy ligand, as discussed above. Similarly, the N−Ru−N angle between the terminal pyridine ring of the ttpy ligand and the isolated pyridine is significantly greater on the side of the methyl group [N(31)−N(41) = 100.0°] than it is on the opposite side [N(31)−N(71) = 84.3°].

MM Calculations. Additional structural information for all of the complexes in solution was obtained from molecular modeling, employing a previously modified MM3* force field[15] in MacroModel.[16] It has been thoroughly demonstrated that well-parametrized MM is substantially more accurate than the third-parametric method (PM3) and other semiempirical methods, and when used in an interpolative sense for steric predictions, MM gives predictions of a quality similar to that of DFT.[17] Parameters to represent the strong homoanomeric effect in pyridyl methanol derivatives were added.[18] The conformational space has been investigated using a low-mode search.[19] The lowest energy conformation of each structure is included in the Supporting Information. According to MM calculations, the structures of both $[Ru(ttpy)(\mathbf{1})]^{2+}$ and $[Ru(ttpy)(\mathbf{2})]^{2+}$ are bent and exist formally in two chiral conformations. However, according to NMR, these conformations are in rapid enantiomeric exchange, making the terminal pyridines of the ttpy ligand equivalent. Of particular interest is the shielding of the H_6 protons of the ttpy ligand, resulting from a close proximity with the central pyridine of the bipyridylpyridyl ligand. In $[Ru(ttpy)(\mathbf{1})]^{2+}$, the distances from H_6 to the center of the orthogonal pyridine are 3.00 and 3.62 Å, respectively, giving an average distance of 3.31 Å and, thus, a fairly strong shielding, in agreement with the NMR. In $[Ru(ttpy)(\mathbf{2})]^{2+}$, because of the higher planarity, the difference is smaller, 3.26 and 3.39 Å, respectively, but the average is similar. In complexes $[Ru(ttpy)(\mathbf{3})]^{2+}$ and $[Ru(ttpy)(\mathbf{4})]^{2+}$, the two H_6 protons are diasterotopic and, thus, separated in the NMR. Because of the homoanomeric effect,[18] the C−O bond will be almost coplanar with both flanking pyridine rings. As a result, the methyl substituent will be almost orthogonal to the pyridine planes, and it will interact strongly with one of the ttpy H_6 protons. In complex $[Ru(ttpy)(\mathbf{3})]^{2+}$, the H_6 proton will be pushed away by the methyl group to a distance of 3.54 Å from the center pyridine and, thus, will experience almost no shielding, whereas the other H_6 proton is located at a distance of only 3.09 Å from the center pyridine and experiences strong shielding. This is in perfect agreement with the NMR results. In complex $[Ru(ttpy)(\mathbf{4})]^{2+}$, the methoxy and methyl groups point in opposite directions, each interacting with one ttpy H_6. The distances to the center pyridine are 3.36 Å and 3.29 Å, respectively, and thus, the shielding difference is much smaller than that for $[Ru(ttpy)(\mathbf{3})]^{2+}$.

Electrochemical Data. The redox properties of the complexes were investigated by cyclic voltammetry in acetonitrile. The $Ru^{III/II}$ redox couples were observed at $E_{1/2}$ = 0.78−0.82 V (vs $Fc^{+/0}$) in all of the complexes except for $[Ru(ttpy)(\mathbf{2})]^{2+}$, which exhibited the $Ru^{III/II}$ redox couple at $E_{1/2}$ = 0.95 V because of the electron-withdrawing carbonyl functionality in ligand **2** (Table 4). Under the same conditions, $[Ru(bpy)_3]^{2+}$ displayed a metal-based oxidation at $E_{1/2}$ = 0.88 V. The ligand-based reductions occurred in a relatively narrow range of potentials except for $[Ru(ttpy)(\mathbf{2})]^{2+}$, which is attributed to the much better π-accepting ability of ligand **2**. A similar shift for the ligand-based reduction in di-(2-pyridyl)-ketone-substituted ruthenium(II) polypyridyl complexes has previously been observed.[20]

UV−Vis Spectroscopy. The absorption spectra of $[Ru(\mathbf{1})_2]^{2+}$, $[Ru(ttpy)(\mathbf{1})]^{2+}$, and $[Ru(ttpy)(\mathbf{2})]^{2+}$ in acetonitrile are shown in Figure 3. The wavelengths of the absorption maxima and the values of the molar absorption coefficients for all of the complexes are listed in Table 4. The spectra in the visible region were dominated by the expected $d \rightarrow \pi^*$ ^{1}MLCT bands and in the UV region by ligand-centered $\pi \rightarrow \pi^*$ transitions.[3,4] The ^{1}MLCT bands in the heteroleptic 4′-tolyl-2,2′:6′,2″-terpyridine-containing complexes are more intense than those for the homoleptic complexes as an effect of the delocalization of the ^{1}MLCT state over the ttpy ligand.[21] In $[Ru(\mathbf{1})_2]^{2+}$, additional features were observed at approximately 410 and 350 nm (Figure 3). The latter can be assigned to $d\pi \rightarrow \pi^*$ (pyridine) transitions by comparison

(14) Lashgari, K.; Kritikos, M.; Norrestam, R.; Norrby, T. *Acta Crystallogr., Sect. C* **1999**, *C55*, 64.
(15) Brandt, P.; Norrby, T.; Åkermark, B.; Norrby, P.-O. *Inorg. Chem.* **1998**, *37*, 4120.
(16) (a) Mohamadi, F.; Richards, N. G. J.; Guida, W. C.; Liskamp, R.; Lipton, M.; Caulfield, C.; Chang, G.; Hendrickson, T.; Still, W. C. *J. Comput. Chem.* **1990**, *11*, 440. (b) *MacroModel*, version 7.2; Schrödinger Inc.: Portland, OR. http://www.schrodinger.com.
(17) Liljefors, T.; Gundertofte, K.; Norrby, P.-O.; Pettersson, I. In *Computational Medicinal Chemistry and Drug Discovery*; Tollenaere, J., de Winter, H., Langenaeker, W., Bultinck, P., Eds.; Marcel Dekker: New York, 2004; pp 1−28.
(18) Norrby, P.-O.; Wärnmark, K.; Åkermark, B.; Moberg, C. *J. Comput. Chem.* **1995**, *16*, 620.
(19) Kolossvary, I.; Guida, W. C. *J. Am. Chem. Soc.* **1996**, *118*, 5011.
(20) Basu, A.; Kasar, T. G.; Sapre, N. Y. *Inorg. Chem.* **1988**, *27*, 4539.
(21) Collin, J.-P.; Guillerez, S.; Sauvage, J.-P.; Barigelletti, F.; De Cola, L.; Flamigni, L.; Balzani, V. *Inorg. Chem.* **1991**, *30*, 4230.

Table 4. Electrochemical and UV−Vis Data in CH_3CN

complex[a]	$E_{1/2}/V^b$ (ΔE_p/mV)[c]		absorption peak wavelength ($\epsilon \times 10^{-4}$, $M^{-1}cm^{-1}$)	
	$Ru^{2+/+}$	$Ru^{3+/2+}$	$d\pi \rightarrow \pi^*$	$\pi \rightarrow \pi^*$
$[Ru(\mathbf{1})_2]^{2+}$	−1.67 (61)	0.78 (73)	477 (0.82)	297 (4.4)
$[Ru(ttpy)(\mathbf{1})]^{2+}$	−1.61 (67)	0.82 (87)	486 (1.5)	297 (5.2), 316 (4.2)
$[Ru(ttpy)(\mathbf{2})]^{2+}$	−1.13 (66)	0.95 (71)	474 (0.87)	282 (3.7), 312 (3.5)
$[Ru(ttpy)(\mathbf{3})]^{2+}$	−1.60 (71)	0.79[d]	482 (1.5)	315 (4.5), 293 (5.8)
$[Ru(ttpy)(\mathbf{4})]^{2+}$	−1.60 (66)	0.81 (89)	482 (1.7)	314 (4.7), 293 (6.2)
$[Ru(tpy)_2]^{2+}$ [e]	−1.62[f]	0.92[f]	476 (1.8)	272 (3.8), 308(6.4)[g]
$[Ru(ttpy)_2]^{2+}$ [e]	−1.62[f]	0.87[f]	490 (2.8)	
$[Ru(bpy)_3]^{2+}$	−1.74 (76)	0.88 (79)	450 (1.4)[h]	288 (7.9)

[a] Complexes as PF_6^- salts. [b] $E_{1/2}$ was taken as the mean value of the anodic and cathodic peak potentials, versus $Fc^{+/0}$, in a CH_3CN solution with 0.1 M $[N(n\text{-}C_4H_9)_4]PF_6$ as the supporting electrolyte, ± 0.02 V. [c] $\upsilon = 100$ mVs^{-1}. [d] Counter peak not observed. [e] From ref 4. [f] Originally reported vs SSCE. 0.375 V is subtracted to obtain values versus $Fc^{+/0}$. [g] From ref 24. [h] From Anderson et al. *Inorg. Chem.* **1995**, *34*, 6145.

Table 5. Emission Properties in Deoxygenated Ethanol/Methanol Solution

	298 K			77 K			
complex[a]	λ_{max} (nm)	τ (ns)	Φ	λ_{max} (nm)	τ (ns)	Φ	$I_{em(0-1)}/I_{em(0-0)}$[b]
$[Ru(\mathbf{1})_2]^{2+}$	655	15.0	1×10^{-3}	609	3720	0.21	0.68
$[Ru(ttpy)(\mathbf{1})]^{2+}$	655	1.4	2×10^{-4}	637	8130	0.21[c]	0.58
$[Ru(ttpy)(\mathbf{2})]^{2+}$				696	1920 (75%) 5840 (25%)	0.11	
$[Ru(ttpy)(\mathbf{3})]^{2+}$	~655	0.14	$\sim 4 \times 10^{-5}$	650	7410	0.30	0.65
$[Ru(ttpy)(\mathbf{4})]^{2+}$	~650	0.47	$\sim 6 \times 10^{-5}$	639	9220	0.31	0.54
$[Ru(tpy)_2]^{2+}$ [d]	*e*	0.25	*e*	598	11000	0.48	0.54[f]
$[Ru(ttpy)_2]^{2+}$ [d]	640	0.95	3.2×10^{-5}	628	9100	*e*	0.53[g]
$[Ru(bpy)_3]^{2+}$ [h]	630	1150	0.089	582	5100	0.33	0.87[g]

[a] Complexes as PF_6^- salts. [b] Intensity ratio of the second over the first vibronic peak in the 77K emission spectrum. See the text for reference and discussion. [c] At 90 K. [d] From ref 4. [e] Not given. [f] From Norrby et al. *Inorg. Chem.* **1997**, *36*, 5850. [g] From ref 9d. [h] From ref 3.

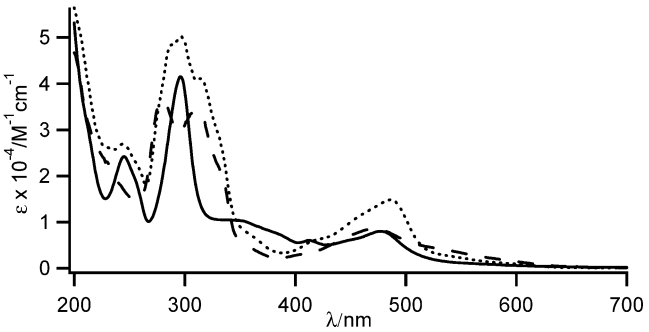

Figure 3. Normalized absorption spectra for $[Ru(\mathbf{1})_2]^{2+}$ (—), $[Ru(ttpy)(\mathbf{1})]^{2+}$ (·····), and $[Ru(ttpy)(\mathbf{2})]^{2+}$ (- - -) in acetonitrile.

with the previously reported $[Ru(bpy)_2(py)_2]^{2+}$.[22] The absorption band at 410 nm can possibly be attributed to a metal-centered transition. The lower energy and higher intensity compared to the metal-centered transitions around 320−340 nm in $[Ru(bpy)_3]^{2+}$ can probably be attributed to the lower symmetry of the new complexes, if our assignment is correct.[3] The ^{1}MLCT band of $[Ru(ttpy)(\mathbf{2})]^{2+}$ was much broader, with a shoulder at approximately 530 nm that most likely corresponds to $d\pi \rightarrow \pi^*$ (**2**) transitions.

Emission Properties. Emission properties at room temperature and 77 K are listed in Table 5. At 77 K, all complexes show a fairly strong emission from the ^{3}MLCT state (Figure 4). The emission maxima are close to or slightly red-shifted relative to $[Ru(ttpy)_2]^{2+}$ for $[Ru(ttpy)(\mathbf{1})]^{2+}$, $[Ru(ttpy)(\mathbf{3})]^{2+}$, $[Ru(ttpy)(\mathbf{4})]^{2+}$, and $[Ru(\mathbf{4})_2]^{2+}$, whereas the excited-state energy is closer to that of $[Ru(tpy)_2]^{2+}$ for $[Ru(\mathbf{1})_2]^{2+}$ ($E_{0-0} = 2.03$ and 2.07 eV for $[Ru(\mathbf{1})_2]^{2+}$ and $[Ru(tpy)_2]^{2+}$, respectively, as estimated from the wavelength maximum of the first vibronic peak in the 77 K spectra). In contrast, the excited-state energy in complex $[Ru(ttpy)(\mathbf{2})]^{2+}$ is much lower in energy because of the π-accepting ligand **2**.

At room-temperature, all of the complexes show a very weak emission, although it should be noted that $[Ru(\mathbf{1})_2]^{2+}$ shows a substantial increase in emission quantum yield compared to the parent complex $[Ru(tpy)_2]^{2+}$. The emission spectra at 77 K for complexes $[Ru(\mathbf{1})_2]^{2+}$ and $[Ru(ttpy)(\mathbf{1})]^{2+}$ display a well-resolved vibronic structure from involvement of medium-frequency ($\nu \sim 1300$ cm^{-1}) stretching modes of the polypyridine ligand.[3,23] The corresponding vibronic progression is less apparent but well resolved in $[Ru(ttpy)(\mathbf{3})]^{2+}$ and $[Ru(ttpy)(\mathbf{4})]^{2+}$.

Temperature-Dependent Emission. At room temperature, both $[Ru(\mathbf{1})_2]^{2+}$ and $[Ru(ttpy)(\mathbf{1})]^{2+}$ show an increased excited-state lifetime compared to $[Ru(tpy)_2]^{2+}$ ($\tau = 0.25$ ns) and $[Ru(ttpy)_2]^{2+}$ ($\tau = 0.95$ ns).[4] The homoleptic $[Ru(\mathbf{1})_2]^{2+}$ complex shows the longest excited-state lifetime: $\tau = 15$ ns in a methanol/ethanol (1:4) solution and $\tau = 17$ ns in acetonitrile. In contrast, $[Ru(ttpy)(\mathbf{3})]^{2+}$ and $[Ru(ttpy)(\mathbf{4})]^{2+}$ show shorter excited-state lifetimes than $[Ru(ttpy)_2]^{2+}$ (Table

(22) (a) Krause, R. A. *Inorg. Chim. Acta*, **1977**, *22*, 209. (b) Sullivan, B. P.; Salmon, D. J.; Meyer, T. J.; Peedin, J. *Inorg. Chem.* **1979**, *18*, 3369.

(23) Meyer, T. J. *Pure Appl. Chem.* **1986**, *58*, 1193.

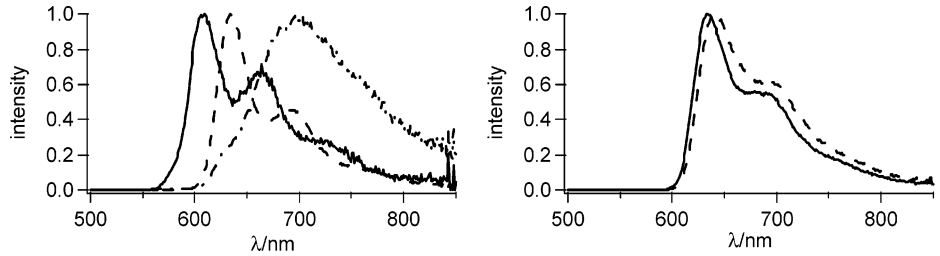

Figure 4. Corrected and normalized emission spectra at 77 K in ethanol/methanol glass. Left: $[Ru(\mathbf{1})_2]^{2+}$ (−), $[Ru(ttpy)(\mathbf{1})]^{2+}$ (− − −) (at 90 K), and $[Ru(ttpy)(\mathbf{2})]^{2+}$ (− · −). Right: $[Ru(ttpy)(\mathbf{3})]^{2+}$ (− − −) and $[Ru(ttpy)(\mathbf{4})]^{2+}$ (−).

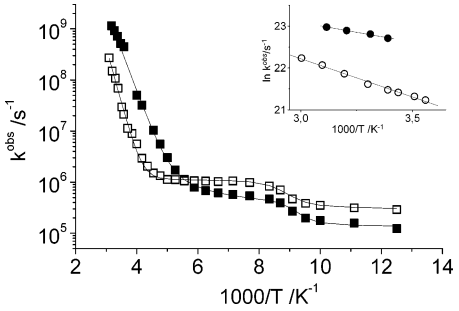

Figure 5. Temperature-dependence of the emission decay rate constant for $[Ru(\mathbf{1})_2]^{2+}$ (□) and $[Ru(ttpy)(\mathbf{1})]^{2+}$ (■). The solid lines are the results of a fit of the data to eq 1. Inset: Temperature-dependence of the emission decay rate constant in the high-temperature region for $[Ru(ttpy)(\mathbf{3})]^{2+}$ (●) and $[Ru(ttpy)(\mathbf{4})]^{2+}$ (○).

5). For $[Ru(ttpy)(\mathbf{2})]^{2+}$, it was not possible to determine a well-defined excited-state lifetime at room temperature.

To better understand the reasons for the excited-state deactivation, the emission lifetime was measured as a function of temperature, in the range 280−333 K for $[Ru(ttpy)(\mathbf{3})]^{2+}$ and $[Ru(ttpy)(\mathbf{4})]^{2+}$ and 90−323 K for the more interesting complexes $[Ru(\mathbf{1})_2]^{2+}$ and $[Ru(ttpy)(\mathbf{1})]^{2+}$. Both $[Ru(\mathbf{1})_2]^{2+}$ and $[Ru(ttpy)(\mathbf{1})]^{2+}$ qualitatively show the same temperature-dependence of the emission properties in this temperature interval. When the temperature is decreased, the emission maximum is, at first, red-shifted, and thereafter, a blue shift is observed as the solvent vitrifies (around 115 K). At the same time, the emission quantum yield and lifetime (Figure 5) increase strongly with decreasing temperature. This is a common behavior for ruthenium(II) polypyridyl complexes.[3]

Discussion

The subtle influence of the structure of the ligands on stability and photophysics was realized at an early state from a comparison of the properties of complexes with the related ligands **1**, **2**, **3**, and **4**. The homoleptic complex $[Ru(\mathbf{1})_2]^{2+}$ had a fairly long excited-state lifetime at room temperature (Table 5). Attempts to prepare a homoleptic complex with the carbonyl-containing ligand **2** failed altogether. To compare the ligands **1**, **2**, **3**, and **4**, the heteroleptic complexes $[Ru(ttpy)(\mathbf{1})]^{2+}$, $[Ru(ttpy)(\mathbf{2})]^{2+}$, $[Ru(ttpy)(\mathbf{3})]^{2+}$, and $[Ru(ttpy)(\mathbf{4})]^{2+}$, where one ligand is 4′-tolyl-2,2′:6′,2″-terpyridine, were also prepared. Again, complex $[Ru(ttpy)(\mathbf{1})]^{2+}$ with ligand **1** showed the longest emission lifetime, $\tau = 1.4$ ns. For complex $[Ru(ttpy)(\mathbf{4})]^{2+}$, this lifetime was reduced by about 70%, and for complex $[Ru(ttpy)(\mathbf{3})]^{2+}$, a further reduction by about 70% was observed (Table 5). Finally, complex $[Ru(ttpy)(\mathbf{2})]^{2+}$ had a weak emission at room temperature with a poorly defined lifetime and wavelength maximum.

To more fully understand the relationship between the structure and photophysics of the complexes, both structural data and photophysical results were analyzed in detail. Because X-ray crystal structures could only be obtained for $[Ru(\mathbf{1})_2]^{2+}$ and $[Ru(ttpy)(\mathbf{3})]^{2+}$ (parts a and b of Figure 2, respectively), the structures of all of the complexes were analyzed by MM calculations. The calculated structures of $[Ru(\mathbf{1})_2]^{2+}$ and $[Ru(ttpy)(\mathbf{3})]^{2+}$ were in excellent agreement with the X-ray structures. The MM calculations suggest that none of the ligands **1**, **3**, or **4** is planar in the complexes. The reason is most probably a combination of steric and electronic effects. It has previously been shown that a hydroxy (or methoxy) group at a methylene group in the 2 (or 6) position of a pyridine ring becomes essentially coplanar with the pyridine ring and oriented away from the ring because of overlap between the antibonding C−O orbital and the σ-N orbital of the pyridine.[18] In complex $[Ru(ttpy)(\mathbf{3})]^{2+}$, this overlap should tend to force the hydroxy group into the same plane as the bipyridine and the pyridine rings and push the methyl group into contact with one of the H_6 protons of the terpyridine ligand. This effect is clearly visible in the X-ray structure, where the angles between the planes of the terpyridine and the bipyridylpyridyl ligand are increased on the side of the methyl group and decreased on the opposite side. As a result, the H_6 of the ttpy ligand is pushed slightly out of the shielding region of the central ring of the bipyridylpyridyl ligand. This is verified by the NMR shift of this proton, 8.10 ppm as compared to 7.63 ppm for the H_6 protons of complex $[Ru(ttpy)(\mathbf{1})]^{2+}$. According to MM calculations, the deformation is smaller in complex $[Ru(ttpy)(\mathbf{4})]^{2+}$, with the methoxy-substituted ligand, as a result of the simultaneous interaction between the methoxy group and the other H_6 of the ttpy ligand, leaving the H_6 protons in similar shielding environments.

To conclude this section, the MM calculations and the X-ray crystal structures show that the pyridine ring of the bipyridylpyridyl ligand is bent out of the plane of the bipyridine. Both this bending and the general deformation of the ligand coordination should contribute to a weakening of the ligand field and a shortening of the excited-state lifetimes of the complexes. The photophysical data support this conclusion (see below).

By close analysis of the shapes of low-temperature emission spectra, information about geometrical differences between the ground and excited states can be obtained, thus

Table 6. Parameters from Fits to Eq 1 for $[Ru(\mathbf{1})_2]^{2+}$, $[Ru(ttpy)(\mathbf{1})]^{2+}$), and Three Reference Compounds and Estimated ΔE_2 Values for $[Ru(ttpy)(\mathbf{3})]^{2+}$and $[Ru(ttpy)(\mathbf{4})]^{2+}$ (See Text)

complex	A_1 (s^{-1})	ΔE_1 (cm^{-1})	A_2 (s^{-1})	ΔE_2 (cm^{-1})	M (s^{-1})	C (K)	T_m (K)
$[Ru(\mathbf{1})_2]^{2+}$ [a]	4.4×10^5	100	1.0×10^{15}	3400	6.9×10^5	3700	115
	(5.5×10^5)	(150)	(1.0×10^{14})	(2900)	(6.7×10^5)	(2700)	
$[Ru(ttpy)(\mathbf{1})]^{2+}$	3.8×10^7	530	1.6×10^{14}	2600	2.5×10^5	3800	110
$[Ru(ttpy)(\mathbf{3})]^{2+}$			1.8×10^{11}	700			
$[Ru(ttpy)(\mathbf{4})]^{2+}$			1.1×10^{12}	1300			
$[Ru(tpy)_2]^{2+}$ [b]	*c*	*c*	1.9×10^{13}	1500	*c*	*c*	*c*
$[Ru(ttpy)_2]^{2+}$ [d]	*c*	*c*	1.9×10^{12}	1600	4.8×10^4	*c*	*c*
$[Ru(bpy)_3]^{2+}$ [e]	2.4×10^6	200	1.3×10^{14}	~4000[f]	*c*	*c*	*c*

[a] Values in parentheses are obtained from a constrained fit with $A_2 = 1.0 \times 10^{14}$ s^{-1}, see text. [b] From Hecker et al. *Inorg. Chem.* **1991**, *30*, 538. [c] Not given. [d] From ref 9d. [e] From Macatangay et al. *Inorg. Chem.* **1996**, *35*, 6823. [f] See, for instance, Macatangay et al. *Inorg. Chem.* **1996**, *35*, 6823; Caspar et al. *Inorg. Chem.* **1983**, *22*, 2444; and Clark et al. *J. Photochem. Photobiol. A* **1997**, *110*, 285.

giving information about the degree of delocalization of the excess electron density. The spectral distortion, as judged from the intensity ratio of the second over the first vibronic peak in the emission spectra at 77 K (see Table 5), is a measure of the difference in equilibrium nuclear geometry between the ground and excited states.[23] Typically, this difference is smaller for a ^{3}MLCT state localized on a terpyridine than that on a bipyridine ligand, because the excess electron density is delocalized over a larger ligand, leading to a smaller geometrical distortion and a lower relative intensity of the second vibronic peak.[24] Consequently, complex $[Ru(ttpy)(\mathbf{1})]^{2+}$, in which the lowest ^{3}MLCT state should be localized on the ttpy ligand, shows a smaller spectral distortion than $[Ru(\mathbf{1})_2]^{2+}$. Complexes $[Ru(ttpy)(\mathbf{3})]^{2+}$ and $[Ru(ttpy)(\mathbf{4})]^{2+}$, which should also have a tolyl-terpyridine-localized ^{3}MLCT excited state, show a somewhat larger spectral distortion than $[Ru(ttpy)(\mathbf{1})]^{2+}$. The steric interactions in the ground state, observed by NMR, also presumably lead to a larger nuclear displacement in the excited state. Interestingly, the spectral distortion for $[Ru(\mathbf{1})_2]^{2+}$ is much smaller than that for $[Ru(bpy)_3]^{2+}$ and, instead, is closer to that for $[Ru(ttpy)_2]^{2+}$.[9d] This suggests that the ^{3}MLCT excited state is somewhat delocalized over the entire bipyridylpyridyl ligand **1**.

By detailed analysis of the photophysical data, the different deactivation pathways involved in the excited-state decay can be understood. For typical ruthenium(II) polypyridyl complexes, the lowest excited state is a ^{3}MLCT state, which actually consists of several close-lying states with different degrees of singlet−triplet mixing and, thus, different intrinsic rates of decay to the ground state.[3,25] They dominate the excited-state decay at lower temperatures {below 150 K for $[Ru(\mathbf{1})_2]^{2+}$ and $[Ru(ttpy)(\mathbf{1})]^{2+}$}. At higher temperatures, an activated and usually irreversible surface crossing from the ^{3}MLCT state to short-lived ligand-field states becomes significant, leading to a rapid and radiationless decay to the ground state. For $[Ru(tpy)_2]^{2+}$ and $[Ru(ttpy)_2]^{2+}$, the decay via ligand-field states dominates the excited-state deactivation at room temperature.

The temperature-dependent emission lifetime data in Figure 5 were fitted to eq 1.[3]

$$\frac{1}{\tau^{obs}} = k_0 + \frac{M}{1 + \exp\left[C\left(\frac{1}{T} - \frac{1}{T_m}\right)\right]} + A_1 e^{-\Delta E_1/RT} + A_2 e^{-\Delta E_2/RT} \quad (1)$$

In this equation, k_0 is the sum of the radiative rate constant, k^{rad}, and the rate constant for nonradiative decay directly to the ground state at 77 K, k^{nr}. Both of these rate constants are usually assumed to be temperature-independent at $T >$ 77 K. The second empirical term describes the increase of the radiative decay as the solvent glass melts. The first Arrhenius term describes a weak temperature-dependence attributed to thermal redistribution between the closely spaced ^{3}MLCT states, with somewhat different properties. The final Arrhenius term is due to the activated decay via the population of ligand-field states, which is the main interest of the present paper and is also the term that dominates the decay at room temperature. The activation energy ΔE_2 for this process in $[Ru(\mathbf{1})_2]^{2+}$ and $[Ru(ttpy)(\mathbf{1})]^{2+}$ was determined from the fit of the data to eq 1 (Figure 5) and is given in Table 6. For $[Ru(ttpy)(\mathbf{3})]^{2+}$ and $[Ru(ttpy)(\mathbf{4})]^{2+}$, the value was estimated from a simple linear (Arrhenius) fit to the data of $\ln(1/\tau)$ versus $1/T$ (283−330 K), a temperature range in which the other terms of eq 1 were negligible. Parameters obtained from the fits of the data are given in Table 6.

A fit to the data for $[Ru(\mathbf{1})_2]^{2+}$ gives a preexponential factor, A_2, of 1×10^{15} s^{-1}, which is too high to be interpreted as only a vibrational frequency for surface crossing.[3] A fit with A_2 constrained to a value of 1×10^{14} s^{-1}, which is similar to the values for $[Ru(ttpy)(\mathbf{1})]^{2+}$ and $[Ru(bpy)_3]^{2+}$, gave a lower value for ΔE_2 (values are given in parentheses in Table 6). The difference between these values can be regarded as a measure of the accuracy of the fit to the data in the high-temperature region (the fits are compared in the Supporting Information). Unfortunately, an extension of the data to temperatures higher than 333 K was not possible, because $[Ru(\mathbf{1})_2]^{2+}$ was not very stable at high temperatures. Nevertheless, the activation energy for $[Ru(\mathbf{1})_2]^{2+}$ is still substantially greater compared to those for $[Ru(ttpy)_2]^{2+}$ and $[Ru(tpy)_2]^{2+}$, irrespective of the selected fitting procedure. Also, complex $[Ru(ttpy)(\mathbf{1})]^{2+}$ shows a substantial increase of the energy difference between the ^{3}MLCT and ligand-field states, as compared to those of the reference complexes $[Ru(ttpy)_2]^{2+}$ and $[Ru(tpy)_2]^{2+}$.

The fact that $[Ru(\mathbf{1})_2]^{2+}$ and $[Ru(ttpy)(\mathbf{2})]^{2+}$ show much higher ΔE_2 values compared to that of $[Ru(ttpy)_2]^{2+}$ is

(24) Coe, B. J.; Thompson, D. W.; Culbertson, C. T.; Schoonover, J. R.; Meyer, T. J. *Inorg. Chem.* **1995**, *34*, 3385.
(25) Hager, G. D.; Crosby, G. A. *J. Am. Chem. Soc.* **1975**, *97*, 7031.

Table 7. Deactivation Rate Constants at Room Temperature and 90K

	298 K				90 K			
complex	k^{rad} (s^{-1})	k^{nr} (s^{-1})	k_1^{act} (s^{-1})	k_2^{act} (s^{-1})	k^{rad} (s^{-1})	k^{nr} (s^{-1})	k_1^{act} (s^{-1})	k_2^{act} (s^{-1})
$[Ru(\mathbf{1})_2]^{2+}$	7.4×10^4	2.2×10^6	2.7×10^5 (2.6×10^5)[a]	6.3×10^7 (7.2×10^7)[a]	6.4×10^4	2.4×10^5	1.6×10^4	~0
$[Ru(ttpy)(\mathbf{1})]^{2+}$	1.4×10^5	6.7×10^7	2.9×10^6	5.0×10^8	3.6×10^4	1.1×10^5	7.7×10^3	~0
$[Ru(ttpy)(\mathbf{3})]^{2+}$	2.9×10^5	7.1×10^9						
$[Ru(ttpy)(\mathbf{4})]^{2+}$	1.2×10^5	2.1×10^9						
$[Ru(tpy)_2]^{2+}$ [b]								
$[Ru(ttpy)_2]^{2+}$ [c]	3.6×10^4	3.2×10^8	*b*	7.9×10^8	*b*	*b*	*b*	*b*
$[Ru(bpy)_3]^{2+}$ [d]	7.2×10^4	4.9×10^5	*b*	7.9×10^5	*b*	*b*	*b*	*b*

[a] Values in parentheses are obtained from a constrained fit with $A_2 = 1.0 \times 10^{14}$ s^{-1}, see text. [b] No data available. [c] From ref 9b. [d] From Clark et al. *J. Photochem. Photobiol. A* **1997**, *110*, 285.

interesting and strongly suggests that the ligand-field strength is increased in these complexes as a result of the more octahedral environment around the ruthenium ion. In contrast to previous approaches to increase the excited-state lifetime of ruthenium(II) bistridentate complexes, the present result is obtained without any substantial lowering of the ^{3}MLCT energy.

If the activation energies for complex $[Ru(ttpy)(\mathbf{3})]^{2+}$ and $[Ru(ttpy)(\mathbf{4})]^{2+}$, on the other hand, are compared with literature values for $[Ru(bpy)_3]^{2+}$, $[Ru(tpy)_2]^{2+}$, and $[Ru(ttpy)_2]^{2+}$, it is clear that in $[Ru(ttpy)(\mathbf{3})]^{2+}$ and $[Ru(ttpy)(\mathbf{4})]^{2+}$, the energy difference between the ^{3}MLCT and ligand-field states is even smaller than for $[Ru(tpy)_2]^{2+}$ and $[Ru(ttpy)_2]^{2+}$. These results could be understood from the NMR data and the MM calculations, which suggest a distorted ground-state geometry and, consequently, a weaker ligand-field. This is also supported by the crystal structure for $[Ru(ttpy)(\mathbf{3})]^{2+}$.

The rate constants for the competing deactivation processes calculated from the experimental data are collected in Table 7. The rate constants for the radiative decay (k^{rad}) and the total nonradiative decay [$k_{tot}^{nr} = (1/\tau^{obs}) - k^{rad}$] were calculated according to eqs 2a and 2b. The activated rate constants $k_1^{act} = A_1 e^{-\Delta E_1/RT}$ and $k_2^{act} = A_2 e^{-\Delta E_2/RT}$ were determined from eq 1.

$$k^{rad} = \frac{\Phi}{\tau^{obs}} \tag{2a}$$

$$k_{tot}^{nr} = \frac{1 - \Phi}{\tau^{obs}} \tag{2b}$$

At low temperatures (90 K), the decay is dominated by nonradiative decay directly to the ground state for both $[Ru(\mathbf{1})_2]^{2+}$ and $[Ru(ttpy)(\mathbf{1})]^{2+}$. In the high-temperature region (room temperature), the activated decay via the ligand-field state is the dominating pathway for $[Ru(\mathbf{1})_2]^{2+}$ and $[Ru(ttpy)(\mathbf{1})]^{2+}$ as well as for the reference complexes $[Ru(ttpy)_2]^{2+}$ and $[Ru(tpy)_2]^{2+}$. However, this deactivation rate has been reduced by 1 and 2 orders of magnitude for $[Ru(\mathbf{1})_2]^{2+}$ compared to those of $[Ru(ttpy)_2]^{2+}$ and $[Ru(tpy)_2]^{2+}$, respectively. The success of our strategy to make the complex more octahedral by introducing tridentate bipyridylpyridyl methane ligands, thus improving the room-temperature photophysical properties, is clear.

In conclusion, this study has given valuable insights of structural effects on the photophysical properties of ruthenium(II) polypyridine complexes. Introducing an extra methylene group between two pyridines of a 2,2′:6′,2″-terpyridine to give a bipyridylpyridyl methane ligand (**1**) appears to increase the ligand-field strength in the corresponding ruthenium(II) complexes $[Ru(\mathbf{1})_2]^{2+}$ and $[Ru(ttpy)(\mathbf{1})]^{2+}$ because of a more octahedral coordination. This results in longer excited-state lifetimes compared to those of the parent $[Ru(tpy)_2]^{2+}$ and $[Ru(ttpy)_2]^{2+}$ complexes but with a preserved energy of the ^{3}MLCT excited state. The potential high reactivity of the excited complex for electron- and energy-transfer reactions was, thus, retained, which has not been the case with previously published strategies based on bistridentate complexes. Adding a methyl and a hydroxy/methoxy substituent on the bridging carbon results in a deformation of the coordination environment, as evident from both NMR data and MM calculations. Characteristic NMR shifts and MM calculations show a deviation from octahedral symmetry in the series of heteroleptic complexes $[Ru(ttpy)(\mathbf{1})]^{2+} < [Ru(ttpy)(\mathbf{4})]^{2+} < [Ru(ttpy)(\mathbf{3})]^{2+}$. This decreases the ligand-field strength, as suggested by the photophysical data, thus decreasing the activation energy for populating the short-lived ligand-field states in the series $[Ru(\mathbf{1})_2]^{2+} < [Ru(ttpy)(\mathbf{1})]^{2+} < [Ru(ttpy)(\mathbf{4})]^{2+} < [Ru(ttpy)(\mathbf{3})]^{2+}$. The excited-state lifetime of the homoleptic complex $[Ru(\mathbf{1})_2]^{2+}$ ($\tau = 15$ ns) represents a great improvement compared to those of common bisterpyridine complexes ($\tau < 1$ ns). Even further improvements are most likely feasible, considering the excited-state lifetime ($\tau = 500$ ns) of the related complex $[Ru(bpy)_2(py)_2]^{2+}$ prepared by Meyer and co-workers.[26] The complex $[Ru(\mathbf{1})_2]^{2+}$ is, thus, a promising starting point for future work aimed at linear donor−acceptor triads.

Experimental Section

X-ray diffraction patterns were recorded with a Stoe IPDS diffractometer on a rotating anode Mo-radiation source with ϕ scans of 1° width. The total rotation range was 200°.

Cyclic voltammetry was carried out with a three-electrode setup in a three-compartment cell connected to an Autolab potentiostat with a GPES electrochemical interface (Eco Chemie). The working electrode was a glassy carbon disk (diameter 3 mm, freshly

(26) Durham, B.; Walsh, J. L.; Carter, C. L.; Meyer, T. J. *Inorg. Chem.* **1980**, *19*, 860.

polished). Potentials were measured versus a nonaqueous Ag/Ag^+ reference electrode (CH Instruments, 10 mM $AgNO_3$ in acetonitrile) with a potential of −0.080 V versus the ferrocenium/ferrocene ($Fc^{+/0}$) couple in acetonitrile. All of the potentials reported here are referenced versus the $Fc^{+/0}$ couple by adding −0.080 V to the potentials measured versus the Ag/Ag^+ electrode. Solutions were prepared from dry acetonitrile (Merck, spectroscopy grade, dried with MS 3 Å) and contained ca. 1 mM analyte and 0.1 M tetrabutylammonium hexafluorophosphate (Fluka, electrochemical grade, dried at 373 K) as supporting electrolyte. The glassware used was oven dried, assembled, and flushed with argon while hot. Before all of the measurements, oxygen was removed by bubbling the stirred solutions with solvent-saturated argon, and the samples were kept under an argon atmosphere during the measurements.

^{1}H NMR spectra were recorded on a Varian (300 or 400 MHz) spectrometer in CD_3CN [ruthenium(II) complexes] or $CDCl_3$ (ligands) solutions.

Mass-spectrometry experiments were done on a Bruker BIFLEX III spectrometer (MALDI-TOF) or on a Bruker Daltonics BioAPEX-94e superconducting 9.4 T FTICR mass spectrometer (Bruker Daltonics, Billerica, MA) (ESI−FTICR MS).

UV−vis absorption spectra were measured on a Hewlett-Packard 8453 instrument or on a Varian Cary 50 UV−vis spectrophotometer.

Steady-state emission measurements were performed on a SPEX-Fluorolog II fluorimeter and corrected for different detector sensitivities at different wavelengths. Temperature-dependent steady-state emission spectra for $[Ru(\mathbf{1})_2]^{2+}$ and $[Ru(ttpy)(\mathbf{1})]^{2+}$ as well as 77 K spectra for $[Ru(ttpy)(\mathbf{2})]^{2+}$, $[Ru(ttpy)(\mathbf{3})]^{2+}$, $[Ru(\mathbf{4})_2]^{2+}$, and $[Ru(ttpy)(\mathbf{4})]^{2+}$ were measured in a variable temperature liquid nitrogen cryostat DN1704, and the temperature was set with an intelligent temperature controller ITC601 (Oxford Instruments).

Time-resolved emission measurements at low temperatures were performed with a frequency-tripled Q-switched Nd:YAG laser from Quantel, producing <10 ns flashes. Excitation light at 460 nm was obtained in an optical parametric oscillator. The emission was detected at a right angle with a monochromator and a P928-type PMT. The PMT output was recorded on a Phillips digital oscilloscope (2 G samples/s) and analyzed with a nonlinear least-squares algorithm with the Applied Photophysics LKS60 software. Each kinetic trace was a sum of 15 individual emission decays, and the emission lifetime at each temperature was determined from the average of at least five traces. Excited-state lifetimes at 77 K were measured in a liquid nitrogen filled coldfinger Dewar. Temperature-dependent excited-state lifetimes for $[Ru(\mathbf{1})_2]^{2+}$ and $[Ru(ttpy)(\mathbf{1})]^{2+}$ were measured using a variable temperature liquid nitrogen cryostat DN1704, and the temperature was set with an intelligent temperature controller ITC601 (Oxford Instruments).

At temperatures higher than 283 K, excited-state lifetimes were determined using a time-correlated single photon counting setup. Excitation was performed with 200 kHz laser pulses of 150-fs width generated in a regenerative amplified Ti:Sapphire system from Coherent. The wavelength used for the experiments was 400 nm, obtained from doubling of the fundamental 800 nm light. The emission light was collected perpendicular to the incoming excitation light. A blue filter before the sample and different red filters after the samples were used to remove unwanted wavelengths. Emitted light was collected by a water-cooled Hammamatsu R38094-5 MCP-PMT. All of the emission measurements were carried out in a 1:4 (v/v) methanol/ethanol mixture in 1 × 1-cm quartz cuvettes. The emission decays were fitted to a single-exponential function using a Simplex algorithm in Microcal Origin, version 5.0.

The temperature-dependent emission lifetime data (Figure 5) were fitted to eq 1 using a nonlinear least-squares fitting procedure in Microcal Origin, version 5.0.

Synthesis. The ligands 6-bromo-2,2′-bipyridine,[27] **1**,[10] and **2**[11] and the complexes $Ru(\mathbf{1})_2$,[10] $Ru(DMSO)_4Cl_2$,[28] and $Ru(ttpy)(DMSO)Cl_2$[29] were prepared as described previously.

1-[6-(2,2′-Bipyridyl)]-1-(2-pyridyl)-ethanol (3). 6-Bromo-2,2′-bipyridine (0.509 g, 2.17 mmol) was dissolved in freshly distilled Et_2O/THF (18 mL, 4:1) under a nitrogen atmosphere, and the temperature was reduced to −78 °C. *n*-BuLi (2.5 M, 0.95 mL, 2.3 mmol) was added dropwise, and the dark-red solution was left for 10 min. 2-Acetylpyridine (0.26 mL, 2.3 mmol) was added dropwise, and the solution was left for 20 min before warming it to room temperature. H_2O was added, and the mixture was extracted twice with Et_2O. The combined organic phases were dried over Na_2SO_4, the solvent was removed, and the residue was purified by column chromatography (silica gel, eluent = EtOAc/hexane 1:2) to give **3** (0.314 g, 52%). ^{1}H NMR ($CDCl_3$, 25 °C): δ 2.05 (s, 3H), 6.58 (s, 1H), 7.12 (ddd, 1H), 7.28 (ddd, 1H), 7.62 (dt, 1H), 7.74−7.84 (m, 4H), 8.28 (m, 1H), 8.45 (d, 1H), 8.51 (m, 1H), 8.65 (m, 1H).

1-[6-(2,2′-Bipyridyl)]-1-methoxy-1-(2-pyridyl)-ethane (4). **3** (0.458 g, 1.65 mmol) and potassium *tert*-butoxide (0.191 g, 1.70 mmol) were added to THF (22 mL) and stirred until all of it was dissolved. CH_3I (0.11 mL, 1.8 mmol) was added dropwise, and the mixture was left under a nitrogen atmosphere for 4 h. Water was added and the mixture extracted with Et_2O. After drying it over Na_2SO_4 and removing the solvent, the residue was purified by column chromatography (silica gel, EtOAc/pentane 1:2) and recrystallized from hexane/EtOAc (6:1) to give **4** (0.310 g, 64%). ^{1}H NMR ($CDCl_3$, 25 °C): δ 2.13 (s, 1H), 3.27 (s, 3H), 7.11 (m, 1H), 7.23 (m, 1H), 7.54 (d, 1H), 7.58 (d, 1H), 7.63 (dt, 1H), 7.73 (dt, 1H), 7.76 (t, 1H), 8.26 (d, 1H), 8.38 (d, 1H), 8.55 (m, 1H), 8.61 (m, 1H).

$[Ru(ttpy)(\mathbf{1})][PF_6]_2$. A solution of $Ru(ttpy)(DMSO)Cl_2$ (0.100 g, 0.17 mmol), silvertriflate (0.087 g, 0.34 mmol), and **1** (0.050 g, 0.2 mmol) in EtOH (40 mL) was refluxed for 10 h under argon. The crude product was chromatographed on silica [eluent = CH_3CN/H_2O/saturated KNO_3 (90:5:1)]. The solvent was removed and the resulting solid dissolved in acetone and precipitated with NH_4PF_6 in water. The red precipitate was collected by filtration, washed with water, and dried (0.053 g, 32%). ^{1}H NMR (CD_3CN, 25 °C): δ 2.55 (s, 3H), 4.97 (s, 2H), 6.97 (t, 1H), 7.13 (t, 1H), 7.24 (t, 2H), 7.1 (d, 1H), 7.34 (d, 1H), 7.58−7.61 (m, 3H), 7.63−7.66 (m, 3H), 7.83 (t, 1H), 7.96 (t, 2H), 8.1−8.14 (m, 3H), 8.33−8.39 (m, 2H), 8.61 (d, 3H), 8.93 (s, 2H). ESI−FTICR MS (*m*/*z*): $[M - PF_6^-]^+$ 817.1 (calcd for $C_{38}H_{30}N_6RuPF_6$: 817.12). Elem Anal. Calcd for $C_{38}H_{30}N_6RuP_2F_{12}$ (%): C, 47.46; H, 3.14; N, 8.74. Found: C, 47.25; H, 3.0; N, 8.35.

$[Ru(\mathbf{4})_2][PF_6]_2$. A solution of $Ru(DMSO)_4Cl_2$ (0.158 g, 0.33 mmol) and **4** (0.191 g, 0.66 mmol) in $EtOH/H_2O$ (2:1, 30 mL) was refluxed for 50 h under nitrogen. Complex $[Ru(\mathbf{4})_2]^{2+}$ was subsequently purified as above (0.157 g, 49%). ESI−FTICR MS (*m*/*z*): $[M - PF_6^-]^+$ 829.14 (calcd for $C_{36}H_{34}N_6O_2RuPF_6$: 829.14), $[M - 2PF_6^- - H^+]^+$ 683.17 (calcd for $C_{36}H_{33}N_6O_2Ru$: 683.17). Elem Anal. Calcd for $C_{36}H_{34}N_6O_2RuP_2F_{12}$ (%): C, 44.41; H, 3.52; N, 8.63. Found: C, 44.20; H, 3.71; N, 8.51.

(27) Norrby, T.; Börje, A.; Zhang, L.; Åkermark, B. *Acta Chem. Scand.* **1998**, *52*, 77.
(28) Evans, I. P.; Spencer, A.; Wilkinson, G. *J. Chem. Soc., Dalton Trans.* **1973**, 204.
(29) Johansson, O.; Borgström, M.; Lomoth, R.; Palmblad, M.; Bergquist, J.; Hammarström, L.; Sun, L.; Åkermark, B. *Inorg. Chem.* **2003**, *42*, 2908.

[Ru(ttpy)(4)][PF_6]$_2$. A solution of Ru(ttpy)(DMSO)Cl_2 (0.144 g, 0.25 mmol) and **4** (0.075 g, 0.26 mmol) in EtOH/H_2O (2:1, 15 mL) was refluxed for 17 h under nitrogen. After chromatography and precipitation as PF_6^- salt, the complex was further purified by recrystallization from a CH_3CN/Et_2O mixture (0.150 g, 60%). ^{1}H NMR (CD_3CN, 25 °C): δ 1.91 (s, 3H), 2.54 (s, 3H), 3.13 (s, 3H), 6.96 (ddd, 1H), 7.11 (ddd, 1H), 7.18 (m, 1H), 7.21 (ddd, 1H), 7.27 (ddd, 1H), 7.43 (m, 1H), 7.46 (m, 1H), 7.58 (d, 2H), 7.72−7.85 (m, 3H), 7.91 (dt, 1H), 7.96 (dt, 1H), 8.03 (m, 1H), 8.11 (d, 2H), 8.40 (m, 1H), 8.46 (t, 1H), 8.56 (m, 1H), 8.58−8.64 (m, 2H), 8.69 (dd, 1H), 8.92 (d, 1H), 8.94 (d, 1H). ESI−FTICR MS (*m*/*z*): [M − PF_6^-]$^+$ 861.15 (calcd for $C_{40}H_{34}N_6ORuPF_6$: 861.15), [M − 2PF_6^- − H^+]$^+$ 715.18 (calcd for $C_{40}H_{33}N_6ORu$: 715.18). Elem Anal. Calcd for $C_{40}H_{34}N_6ORuP_2F_{12}$ (%): C, 47.77; H, 3.41; N, 8.36. Found: C, 47.57; H, 3.44; N, 8.37.

[Ru(ttpy)(3)][PF_6]$_2$. A solution of Ru(ttpy)(DMSO)Cl_2 (0.159 g, 0.28 mmol) and **3** (0.080 g, 0.25 mmol) in EtOH/H_2O (2:1, 15 mL) was refluxed for 23 h under nitrogen and isolated as complex [Ru(ttpy)(**1**)] above. Complex [Ru(ttpy)(**3**)] was redissolved in acetone and once more precipitated with NH_4PF_6 in water (0.159 g, 57%). Anion metathesis to the ClO_4^- salt was performed by dissolving the PF_6^- salt in acetone followed by precipitation with a saturated aqueous solution of $NaClO_4$. X-ray quality crystals were obtained by the diffusion of diethyl ether into a CH_3CN solution of Ru(ttpy)(**3**) as ClO_4^- salt. ^{1}H NMR (CD_3CN, 25 °C): δ 1.75 (s, 3H), 2.53 (s, 3H), 6.63 (s, 1H), 6.87 (ddd, 1H), 7.04−7.12 (m, 3H), 7.18 (m, 1H), 7.33 (ddd, 1H), 7.40 (m, 1H), 7.58 (d, 2H), 7.68 (ddd, 1H), 7.76−7.86 (m, 2H), 8.01 (dt, 1H), 8.08−8.15 (m, 3H), 8.26 (m, 1H), 8.37 (m, 1H), 8.41 (t, 1H), 8.49 (m, 1H), 8.63 (dd, 1H), 8.69 (m, 1H), 8.83 (dd, 1H), 8.89 (d, 1H), 8.99 (d, 1H). MALDI-TOF MS (*m*/*z*): [M − 2PF_6^- − H^+]$^+$ 701.04 (calcd for $C_{39}H_{31}N_6ORu$: 701.16). Elem Anal. Calcd for $C_{39}H_{32}N_6ORuP_2F_{12}$ (%): C, 47.23; H, 3.25; N, 8.47. Found: C, 47.14; H, 3.37; N, 8.43.

[Ru(ttpy)(2)][PF_6]$_2$. This complex was prepared and purified in the same way described for complex [Ru(ttpy)(**1**)] above. A solution of Ru(ttpy)(DMSO)Cl_2 (0.065 g, 0.11 mmol), silvertriflate (0.056 g, 0.22 mmol), and **2** (0.030 g, 0.11 mmol) in EtOH (40 mL) was refluxed for 24 h under argon (0.031 g, 28%). ^{1}H NMR (CD_3CN, 25 °C): δ 2.55 (s, 3H), 7.20−7.29 (m, 4H), 7.32 (d, 1H), 7.59−7.63 (m, 3H), 7.66 (d, 2H), 7.86−7.93 (m, 2H), 7.97 (t, 2H), 8.13 (d, 2H), 8.43 (d, 1H), 8.48 (d, 1H), 8.53 (t, 1H), 8.65 (d, 2H), 8.89 (dd, 2H), 8.96 (s, 2H). ESI−FTICR MS (*m*/*z*): [M − PF_6^-]$^+$ 831.1 (calcd for $C_{38}H_{28}N_6ORuPF_6$: 831.10). Elem Anal. Calcd for $C_{38}H_{28}N_6ORuP_2F_{12}$ (%): C, 46.78; H, 2.89; N, 8.61. Found: C, 46.99; H, 3.02; N, 8.39.

Acknowledgment. We thank the Knut and Alice Wallenberg Foundation, the Swedish Research Council, and the Swedish Energy Agency for financial support. L.H. gratefully acknowledges a Research Fellow position from the Royal Swedish Academy of Sciences.

Supporting Information Available: The lowest energy conformation of each structure from the MM calculations and the comparison between the different fit procedures of the temperature-dependent time-resolved emission. This material is available free of charge via the Internet at http://pubs.acs.org.

IC048247A